Electronic Supplementary Material (ESI) for Journal of Materials Chemistry A.

Electronic Supplementary Information

Stannate Derived Bimetallic Nanoparticles for Electrocatalytic CO_2 Reduction

Xiaolong Zhang,[a] Fengwang Li,[a,b] Ying Zhang,[a,b] Alan M. Bond,[a,b] Jie Zhang[a,b]*

[a]School of Chemistry, Monash University, Clayton 3800, Victoria, Australia.

[b]ARC Centre of Excellence for Electromaterials Science, Monash University, Clayton 3800, Victoria, Australia.

*Email: jie.zhang@monash.edu

Figure S1. Powder XRD patterns of metal stannates calcined at 350 °C.

Figure S2. Powder XRD pattern of the Mn-Sn bimetallic catalyst derived from $MnSnO_3$ (black trace) and the standard JCPDS pdf card of $MnSn_2$ (65-2701) and Sn (89-4898).

Figure S3. Powder XRD pattern of the Co-Sn bimetallic catalyst derived from $CoSnO_3$ (black trace) and the standard JCPDS pdf card of CoSn (65-6225).

Figure S4. Powder XRD pattern of the Ni-Sn bimetallic catalyst derived from $NiSnO_3$ (black trace) and the standard JCPDS pdf card of Ni_3Sn (65-9703) and Sn (89-4898).

Figure S5. Powder XRD pattern of the Cu-Sn bimetallic catalyst derived from $CuSnO_3$ (black trace) and the standard JCPDS pdf card of CuSn (65-3434).

Figure S6. Powder XRD pattern of the Zn-Sn bimetallic catalyst derived from $ZnSnO_3$ (black trace) and the standard JCPDS pdf card of Zn (65-5973) and Sn (89-4898).

Figure S7. Powder XRD pattern of the Ag-Sn bimetallic catalyst derived from Ag_2SnO_3 (black trace) and the standard JCPDS pdf card of Ag_3Sn (71-530) and Sn (89-4898).

Figure S8. Powder XRD pattern of the Cd-Sn bimetallic catalyst derived from $CdSnO_3$ (black trace) and the standard JCPDS pdf card of Cd (85-1328) and Sn (89-4898).

Figure S9. Powder XRD pattern of the Pb-Sn bimetallic catalyst derived from $PbSnO_3$ (black trace) and the standard JCPDS pdf card of Pb (87-663) and Sn (89-4898).

Figure S10. Cyclic voltammetry at Metal-Sn bimetallic catalyst modified GC disc electrodes in a CO_2 saturated 0.5M $NaHCO_3$ solution.

Figure S11. Selected area diffraction of Cu-Sn (a) and Ag-Sn (b).

Figure S12. Partial current distribution as a function of applied potential for the Cu-Sn (a) and Ag-Sn (b) catalysts in a CO_2 saturated 0.5M $NaHCO_3$ aqueous solution.

Figure S13. TEM images of Ag_2SnO_3/GO (a,b) and $CuSnO_3$/GO (c,d).

Figure S14. TEM images of Cu-Sn/rGO (a,b) and Ag-Sn/rGO (c,d) after electrolysis.

Table S1. Comparison of Sn based formate-selective CO_2 reduction catalysts in literature.

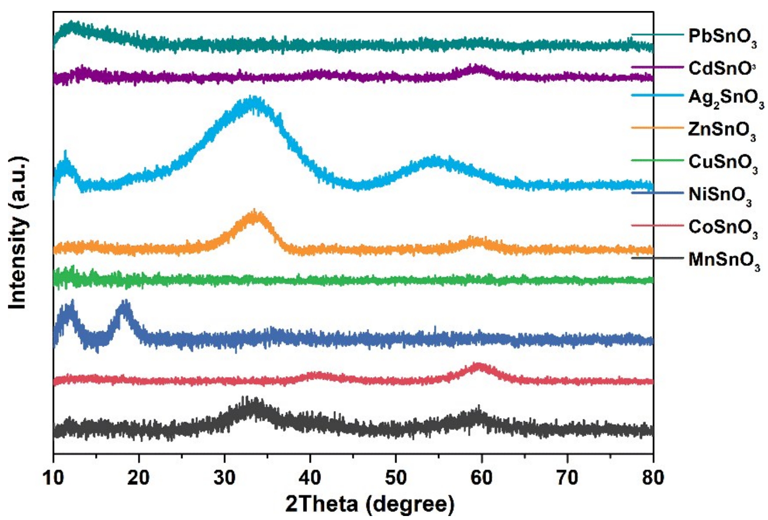

Figure S1. Powder XRD patterns of metal stannates calcined at 350 °C.

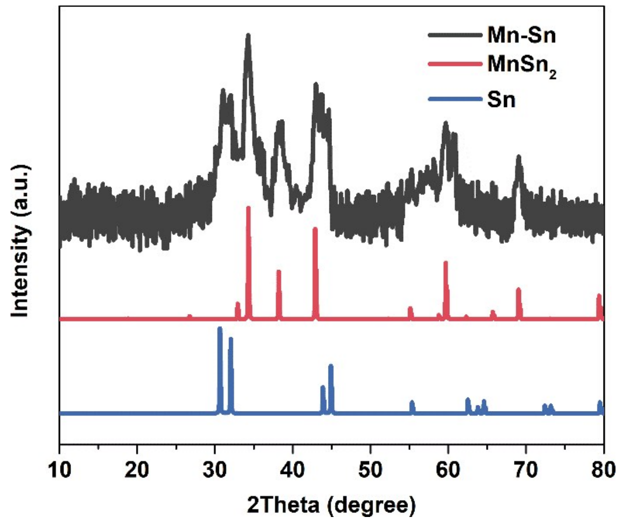

Figure S2. Powder XRD pattern of the Mn-Sn bimetallic catalyst derived from $MnSnO_3$ (black trace) and the standard JCPDS pdf card of $MnSn_2$ (65-2701) and Sn (89-4898).

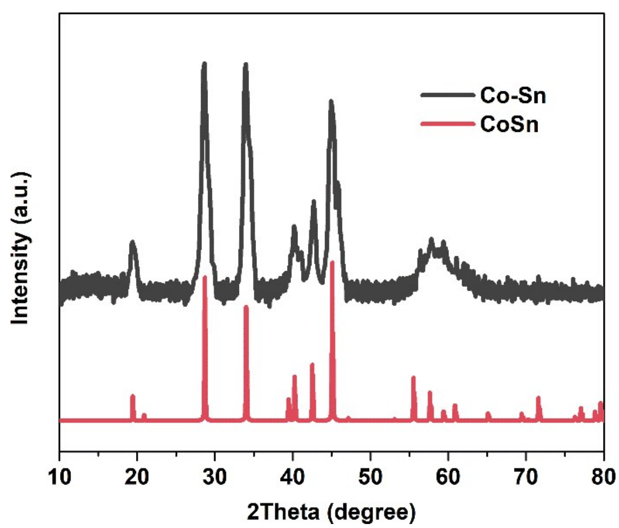

Figure S3. Powder XRD pattern of the Co-Sn bimetallic catalyst derived from $CoSnO_3$ (black trace) and the standard JCPDS pdf card of CoSn (65-6225).

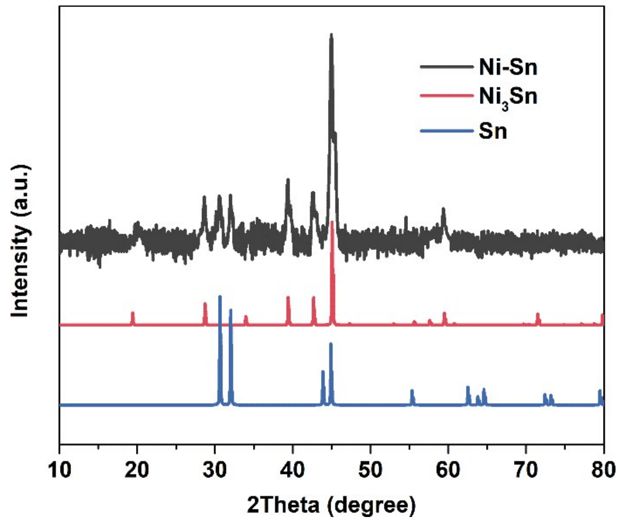

Figure S4. Powder XRD pattern of the Ni-Sn bimetallic catalyst derived from $NiSnO_3$ (black trace) and the standard JCPDS pdf card of Ni_3Sn (65-9703) and Sn (89-4898).

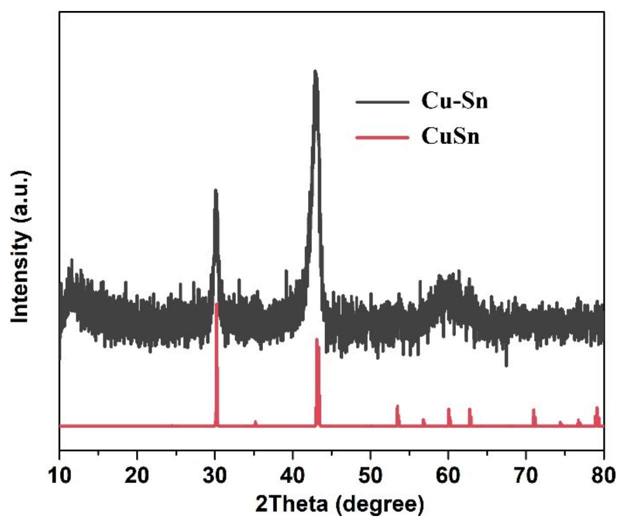

Figure S5. Powder XRD pattern of the Cu-Sn bimetallic catalyst derived from $CuSnO_3$ (black trace) and the standard JCPDS pdf card of CuSn (65-3434).

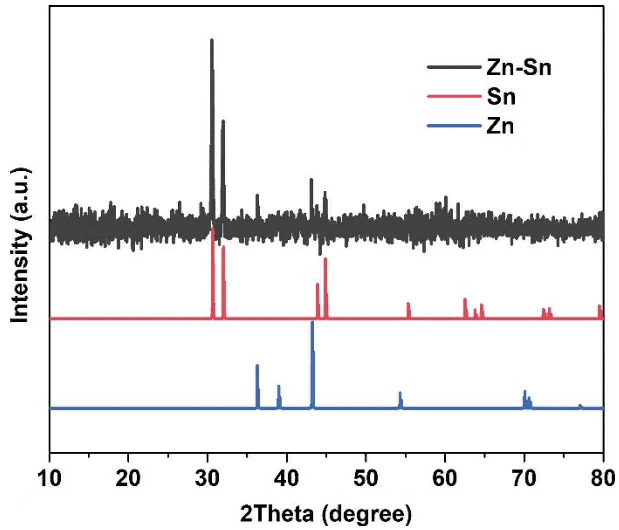

Figure S6. Powder XRD pattern of the Zn-Sn bimetallic catalyst derived from $ZnSnO_3$ (black trace) and the standard JCPDS pdf card of Zn (65-5973) and Sn (89-4898).

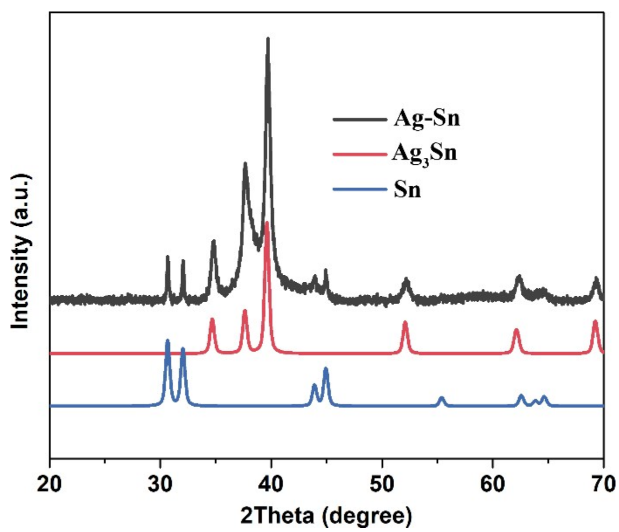

Figure S7. Powder XRD pattern of the Ag-Sn bimetallic catalyst derived from Ag_2SnO_3 (black trace) and the standard JCPDS pdf card of Ag_3Sn (71-530) and Sn (89-4898).

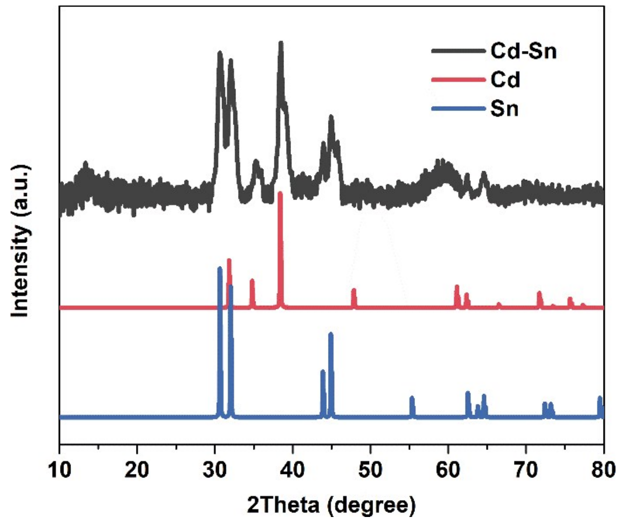

Figure S8. Powder XRD pattern of the Cd-Sn bimetallic catalyst derived from $CdSnO_3$ (black trace) and the standard JCPDS pdf card of Cd (85-1328) and Sn (89-4898).

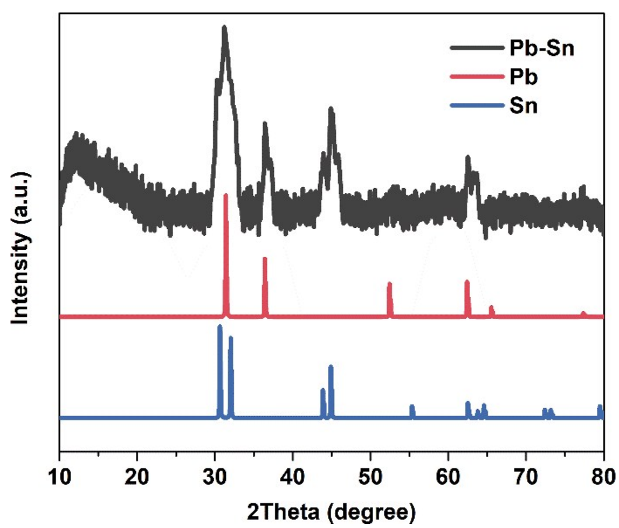

Figure S9. Powder XRD pattern of the Pb-Sn bimetallic catalyst derived from $PbSnO_3$ (black trace) and the standard JCPDS pdf card of Pb (87-663) and Sn (89-4898).

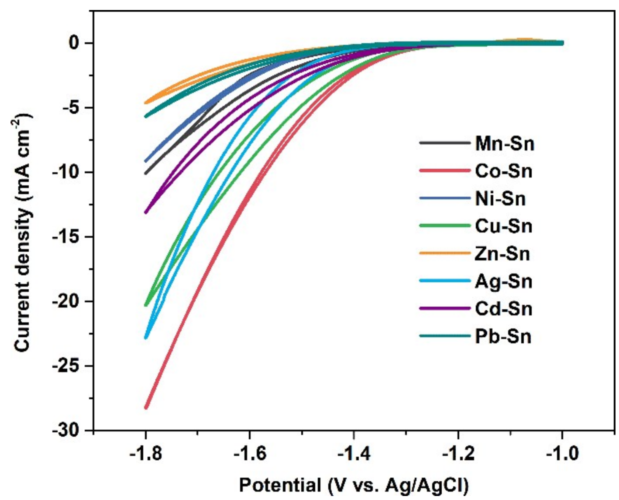

Figure S10. Cyclic voltammetry at metal-Sn bimetallic catalyst modified GC disc electrodes in a CO_2 saturated 0.5M $NaHCO_3$ solution.

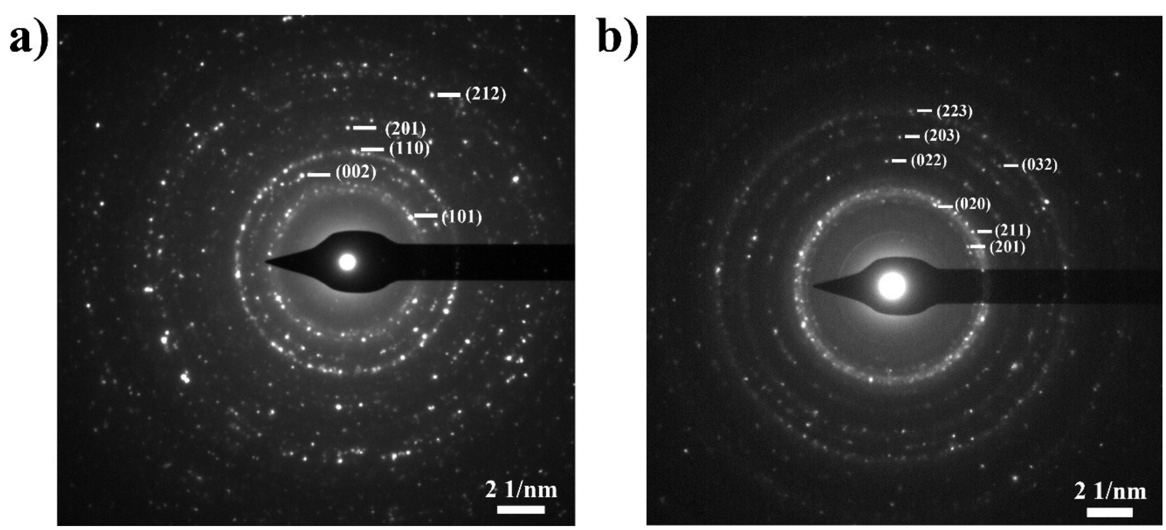

Figure S11. Selected area diffraction of Cu-Sn (a) and Ag-Sn (b).

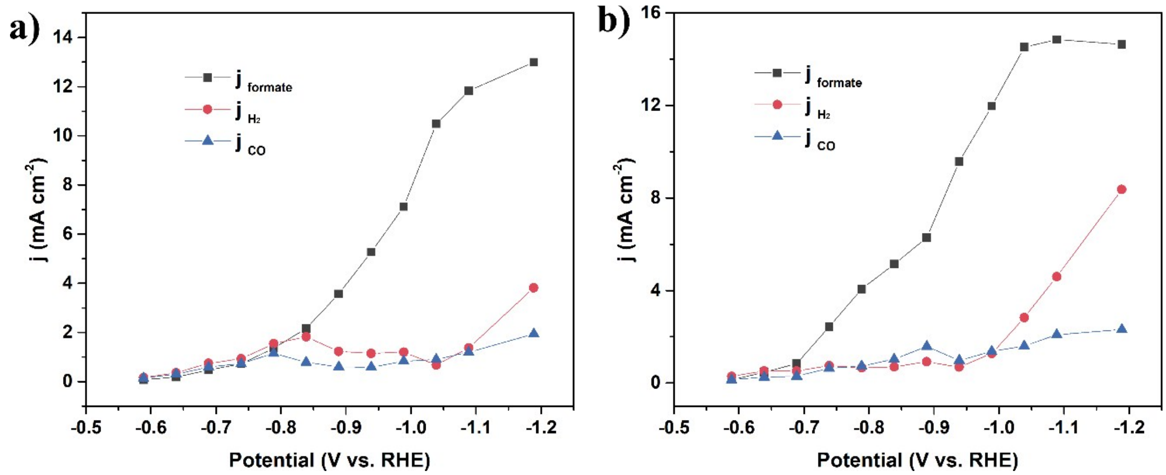

Figure S12. Partial current distribution as a function of applied potential for the Cu-Sn (a) and Ag-Sn (b) catalysts in a CO_2 saturated 0.5M $NaHCO_3$ aqueous solution.

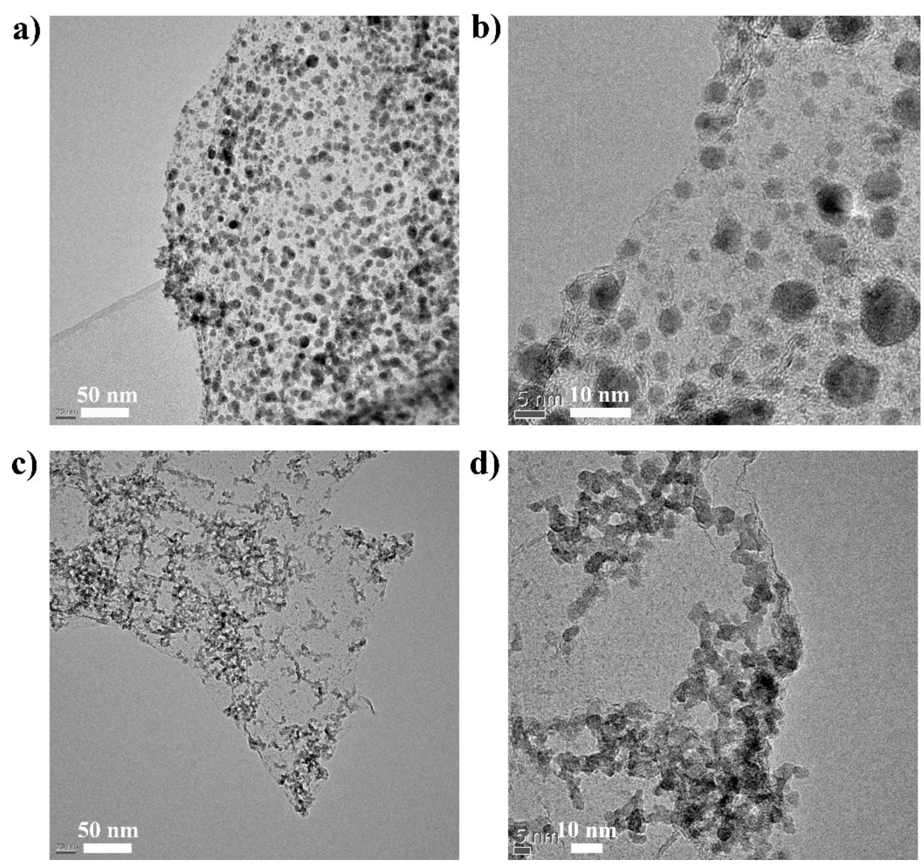

Figure S13. TEM images of Ag_2SnO_3/GO (a,b) and $CuSnO_3$/GO (c,d).

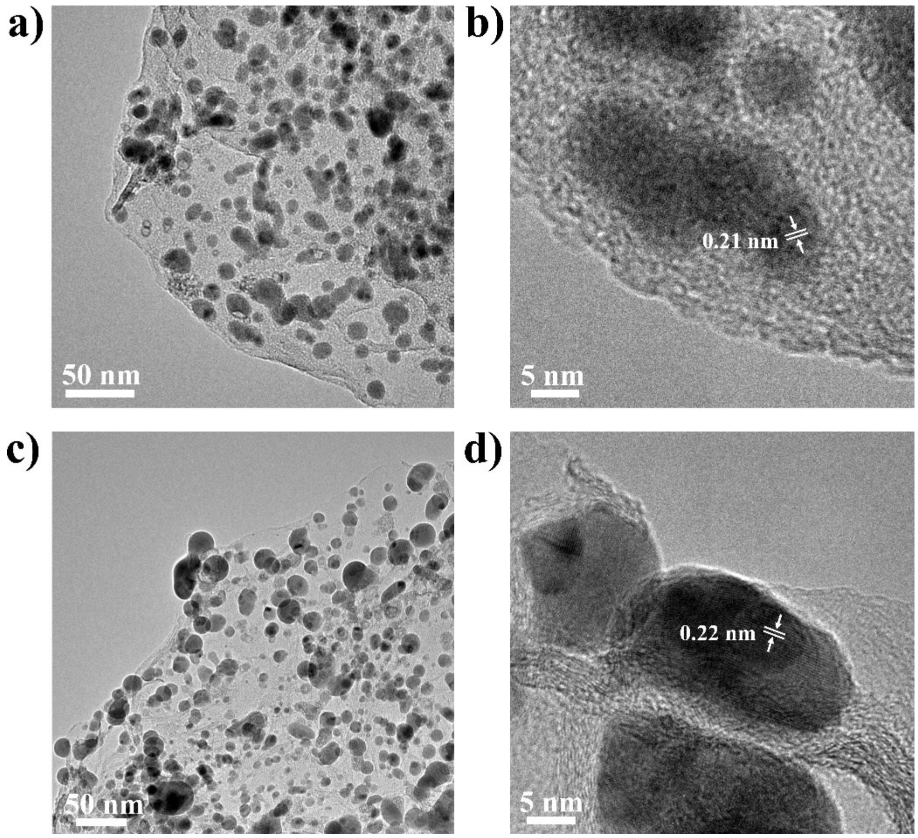

Figure S14. TEM images of Cu-Sn/rGO (a,b) and Ag-Sn/rGO (c,d) after electrolysis.

Table S1. Comparison of our catalysts with Sn based formate-selective CO_2 reduction catalysts reported in literature.

Catalyst	Electrolyte	Potential	Maximum $FE_{formate}$ (%)	Current density (mA cm^{-2})	Electrode substrate	Ref.
Stannate derived Cu-Sn	0.5 M $NaHCO_3$	-1.04 V vs. RHE	86	10.4	Glassy carbon plate	This work
Stannate derived Ag-Sn	0.5 M $NaHCO_3$	-0.94 V vs. RHE	85	9.6	Glassy carbon plate	This work
Cu-Sn/rGO	0.5 M $NaHCO_3$	-0.99 V vs. RHE	87	23.6	Glassy carbon plate	This work
Ag-Sn/rGO	0.5 M $NaHCO_3$	-0.94 V vs. RHE	88	21.3	Glassy carbon plate	This work
$Ag_{76}Sn_{24}$	0.5 M $NaHCO_3$	-0.8 V vs. RHE	80	15.6	Carbon paper	1
Sn dendrite	0.1 M $KHCO_3$	-1.36 V vs. RHE	71.6	17.1	Sn foil	2
Electrodeposited $Sn_{56.3}Pb_{43.7}$	0.5 M $KHCO_3$	-1.36 V vs. RHE	78.8	57.3	Carbon paper	3
Mesoporous SnO_2	0.5 M $NaHCO_3$	-1.0 V vs. RHE	87	45	Carbon cloth	4
Sn/SnO_x	0.5 M $NaHCO_3$	-0.7 V vs. RHE	58	1.8	Sn plate	5
Sn/graphene	0.1 M $NaHCO_3$	-1.16 V vs. RHE	89	21.1	Glassy carbon plate	6
Polycrystalline Sn	0.1 M $KHCO_3$	-1.08 V vs. RHE	58	5	N/A	7
$[Fe_4N(CO)_{12}]^-$	0.1 M $KHCO_3$	-1.2 V vs. SCE	96	3.8	Glassy carbon	8
$IrHL(S)_2$	5:95 v/v H_2O/MeCN	-1.65 V vs. SCE	93	0.6	Glassy carbon	9
$[CpCo(P^R{}_2NR'_2)I]^+$	DMF/water	-2.2 V vs. Fc/Fc^+	90 ± 10	~3	Glassy carbon	10

Reference

1. W. Luc, C. Collins, S. Wang, H. Xin, K. He, Y. Kang and F. Jiao, *Journal of the American Chemical Society*, 2017, **139**, 1885-1893.
2. D. H. Won, C. H. Choi, J. Chung, M. W. Chung, E.-H. Kim and S. I. Woo, *ChemSusChem*, 2015, **8**, 3092-3098.
3. S. Y. Choi, S. K. Jeong, H. J. Kim, I. H. Baek and K. T. Park, *Acs Sustainable Chemistry & Engineering*, 2016, **4**, 1311-1318.
4. F. Li, L. Chen, G. P. Knowles, D. R. MacFarlane and J. Zhang, *Angew Chem Int Ed Engl*, 2017, **56**, 505-509.
5. Y. Chen and M. W. Kanan, *Journal of the American Chemical Society*, 2012, **134**, 1986-1989.
6. F. Lei, W. Liu, Y. Sun, J. Xu, K. Liu, L. Liang, T. Yao, B. Pan, S. Wei and Y. Xie, *Nature Communications*, 2016, **7**, 12697.

7. Y. Hori, H. Wakebe, T. Tsukamoto and O. Koga, *Electrochimica Acta*, 1994, **39**, 1833-1839.

8. A. Taheri, E. J. Thompson, J. C. Fettinger and L. A. Berben, *ACS Catalysis*, 2015, **5**, 7140-7151.

9. P. Kang, C. Cheng, Z. Chen, C. K. Schauer, T. J. Meyer and M. Brookhart, *Journal of the American Chemical Society*, 2012, **134**, 5500-5503.

10. S. Roy, B. Sharma, J. Pécaut, P. Simon, M. Fontecave, P. D. Tran, E. Derat and V. Artero, *Journal of the American Chemical Society*, 2017, **139**, 3685-3696.